

Boosted Self-interacting Dark Matter in a Multi-component Dark Matter Model

Mayumi Aoki^{1*}, Takashi Toma^{2†}

¹*Institute for Theoretical Physics, Kanazawa University, Kanazawa 920-1192, Japan*

²*Physik-Department T30d, Technische Universität München,
James-Frank-Straße, D-85748 Garching, Germany*

Abstract

In models of multi-component dark matter, the lighter component of dark matter can be boosted by annihilations of the heavier state if mass splitting is large enough. Such relativistic dark matter can be detectable via large neutrino detectors such as Super-Kamiokande and IceCube. Moreover, if the process is inelastic scattering and decay length of the produced particle is short enough, another signature coming from the decay can also be detectable. In this paper, we construct a simple two-component dark matter model with a hidden $U(1)_D$ gauge symmetry where the lighter component of dark matter has a potential to improve the so-called small scale structure problems with large self-interacting cross section. We estimate number of multi-Cherenkov ring events due to both of the boosted dark matter and subsequent decay of the particle produced by inelastic scattering at Hyper-Kamiokande future experiment. Some relevant constraints, such as dark matter direct detection and cosmological observations, are also taken into account. The numerical analysis shows that some parameter space which can induce large self-interacting cross section can give a few multi-Cherenkov ring events per year at Hyper-Kamiokande.

*mayumi@hep.s.kanazawa-u.ac.jp

†takashi.toma@tum.de

1 Introduction

From cosmological observations, it is clear that dark matter exists in the universe. However our knowledge about dark matter is limited. We know that 26% of the total energy density in the universe is occupied by dark matter [1], but the nature of the particle of dark matter, mass and interaction other than gravity are unknown. Revealing the nature of dark matter is one of the most important issues in (astro-)particle physics.

From the point of view of dark matter model building, many models have been proposed so far, and in those models one component dark matter is often considered just for simplicity. Exploring the simplest possibility at first would actually be the best option. However there is no strong motivation to consider only one component dark matter. In fact, multi-component dark matter naturally appears and is phenomenologically motivated in some cases [2–17], and some interesting consequences are expected such as double disk galaxy structure constructed by normal matter and dark matter [18, 19], multiple gamma-ray line signals and boosted dark matter signals [20–26] and so on.

In particular, boosted dark matter is an interesting consequence of multi-component dark matter though it can also be produced by dark matter semi-annihilations or decay of a long-lived particle for example [20–26]. If the heavier component of dark matter annihilates into the lighter dark matter with a certain cross section, the produced lighter dark matter has a large momentum, namely it is boosted. The boosted dark matter behaves as relativistic neutrinos and may be detected by large neutrino detectors such as Super-Kamiokande [27, 28], IceCube [29, 30], and future experiments Hyper-Kamiokande [31], PINGU [32] and DUNE [33] through (in)elastic scattering with electrons or protons in detectors. If the process is inelastic scattering and the decay length of the particle produced by this scattering is shorter than detector length, another signal can be expected [23]. This can be a characteristic signature of multi-component dark matter, or in other words non-minimal dark sector.

In this paper, we construct a UV-complete model including two-component dark matter with a hidden $U(1)_D$ gauge symmetry. We introduce three new scalar fields and one of these fields has a milli-charge of the hidden $U(1)_D$ gauge symmetry. After the spontaneous symmetry breaking, two hidden particles can be stable because of the residual $\mathbb{Z}_2 \times \mathbb{Z}'_2$ symmetry. The lighter component of dark matter has potential to solve small scale structure problems [34, 35], such as cusp-vs-core problem, too-big-to-fail problem and missing satellite problem, with large self-interacting cross section. This model is regarded as a variant of the model which has been investigated in the literature [36]. The field content is exactly the same, but a difference is that one of the new particles is milli-charged under the $U(1)_D$ symmetry. We explore parameter space inducing the signatures of boosted dark matter in the two-component dark matter model concerning some relevant constraints such as dark matter relic abundance, direct detection, cosmic-ray and cosmological observations, perturbativity of couplings, and we estimate number of multi-Cherenkov ring events originated from boosted dark matter coming from the

Table 1: Particle content and charge assignment where Q_χ is an arbitrary value consistent with Eq. (1) and (2). All the new particles are scalar fields.

	Σ	S	χ
Q_D	1	-1/2	Q_χ
Remnant $\mathbb{Z}_2 \times \mathbb{Z}'_2$	(0, 0)	(1, 0)	(0, 1)

Galactic centre which can be detectable at Hyper-Kamiokande future experiment.

The paper is organized as follows. In the next Section, the model is presented in detail. In Section 3, quantitative treatments of boosted dark matter will be discussed. Section 4 is devoted to describe the relevant constraints, and numerical calculations will be done in Section 5. Conclusion and summary is given in Section 6.

2 The Model

We consider the model extended by a hidden $U(1)_D$ gauge symmetry with three new scalar fields Σ , S and χ as shown in Tab. 1. This model is a variant of the previous model which has been considered in the literature [36]. Unlike the previous case, we take arbitrary hidden $U(1)_D$ charge for χ consistent with the following Lagrangian (e.g. $Q_\chi = 1/5, 2/5, \dots$) so that the $\mathbb{Z}_2 \times \mathbb{Z}'_2$ symmetry remains after symmetry breaking. The kinetic terms of the new scalar fields are given by

$$\mathcal{L} = |D_\mu \Sigma|^2 + |D_\mu S|^2 + |D_\mu \chi|^2 - \frac{\epsilon}{2} B_{\mu\nu} Z'^{\mu\nu}, \quad (1)$$

where ϵ is the kinetic mixing between the Standard Model $U(1)_Y$ and the hidden $U(1)_D$ symmetries. The full scalar potential is written down as

$$\begin{aligned} \mathcal{V} = & \mu_\Phi^2 |\Phi|^2 + \mu_\Sigma^2 |\Sigma|^2 + \mu_S^2 |S|^2 + \mu_\chi^2 |\chi|^2 + \frac{\lambda_\Phi}{4} |\Phi|^4 + \frac{\lambda_\Sigma}{4} |\Sigma|^4 + \frac{\lambda_S}{4} |S|^4 + \frac{\lambda_\chi}{4} |\chi|^4 \\ & + \lambda_{\Phi\Sigma} |\Phi|^2 |\Sigma|^2 + \lambda_{\Phi S} |\Phi|^2 |S|^2 + \lambda_{\Phi\chi} |\Phi|^2 |\chi|^2 + \lambda_{\Sigma S} |\Sigma|^2 |S|^2 + \lambda_{\Sigma\chi} |\Sigma|^2 |\chi|^2 + \lambda_{S\chi} |S|^2 |\chi|^2 \\ & + \left(\frac{\kappa}{2} \Sigma S^2 + \text{H.c.} \right). \end{aligned} \quad (2)$$

In addition to the above scalar potential, the following terms

$$\mathcal{V}' = \left(\frac{\mu}{2} S \chi^2 + \frac{\lambda}{2} \Sigma S \chi^{\dagger 2} + \text{H.c.} \right), \quad (3)$$

can also be allowed if $Q_\chi = 1/4$.¹ In this case, the model results in the previous model [36]. As we will see later, χ and the CP-odd component of S can be identified as dark matter candidates simultaneously, and we focus on the dark matter mass less than $\mathcal{O}(10)$ GeV. In this mass range, the magnitude of the $U(1)_D$ charge should be $Q_\chi g_D \lesssim 10^{-2}$ in order

¹ $Q_\chi = -1/4$ also gives the same additional terms with Eq. (3) obtained by exchanging $\chi \leftrightarrow \chi^\dagger$.

to be consistent with the observed relic abundance and direct detection of dark matter.² Thus the terms in Eq. (3) are eventually forbidden. Hereafter the couplings $\lambda_{\Phi\chi}$ and $\lambda_{\Sigma\chi}$ are set to be zero for simplicity. Practically, these couplings should satisfy $\lambda_{\Phi\chi}\sin^2\alpha + \lambda_{\Sigma\chi}\cos^2\alpha \lesssim 10^{-4}(m_\chi/\text{GeV})$ not to affect our following analysis (not too deplete relic abundance of χ).

The hidden $U(1)_D$ gauge symmetry is spontaneously broken by the vacuum expectation value of Σ which is parametrized as $\Sigma = \langle\Sigma\rangle + \sigma/\sqrt{2}$, and the hidden gauge boson Z' gets the mass $m_{Z'} \equiv g_D\langle\Sigma\rangle$. Similarly, the Higgs doublet field is written as $\Phi = (0, \langle\Phi\rangle + \phi^0/\sqrt{2})^T$ in the Unitary gauge. The gauge eigenstates ϕ^0 and σ mix with each other via the coupling $\lambda_{\Phi\Sigma}$, and these gauge eigenstates can be rewritten as

$$\begin{pmatrix} \phi^0 \\ \sigma \end{pmatrix} = \begin{pmatrix} \cos\alpha & -\sin\alpha \\ \sin\alpha & \cos\alpha \end{pmatrix} \begin{pmatrix} h \\ H \end{pmatrix}, \quad \text{with} \quad \sin 2\alpha = \frac{4\lambda_{\Phi\Sigma}\langle\Phi\rangle\langle\Sigma\rangle}{m_h^2 - m_H^2}, \quad (4)$$

where the mass eigenstates h and H correspond to the SM-like Higgs boson with $m_h = 125$ GeV and the second extra Higgs boson, respectively. With the orthogonal matrix given in Eq. (4), one can rewrite the quartic couplings λ_Φ and λ_Σ as

$$\lambda_\Phi = \frac{1}{\langle\Phi\rangle^2} (m_h^2 \cos^2\alpha + m_H^2 \sin^2\alpha), \quad (5)$$

$$\lambda_\Sigma = \frac{1}{\langle\Sigma\rangle^2} (m_h^2 \sin^2\alpha + m_H^2 \cos^2\alpha). \quad (6)$$

The complex scalar field $S = (s + ia)/\sqrt{2}$ splits into the CP-even and CP-odd mass eigenstates s and a whose masses are given by

$$m_s^2 = \mu_S^2 + \lambda_{\Sigma S}\langle\Sigma\rangle^2 + \kappa\langle\Sigma\rangle, \quad (7)$$

$$m_a^2 = \mu_S^2 + \lambda_{\Sigma S}\langle\Sigma\rangle^2 - \kappa\langle\Sigma\rangle. \quad (8)$$

Thus the squared mass difference is given by $m_s^2 - m_a^2 = 2\kappa\langle\Sigma\rangle$. Since we can take $\kappa > 0$ without loss of generality, this means $m_s > m_a$.

The gauge kinetic mixing $\epsilon_\gamma \equiv \epsilon \cos\theta_W$ is experimentally constrained by $Z' \rightarrow e^+e^-$ search and the current exclusion limits on the kinetic mixing ϵ_γ are summarized in Fig. 1 including beam dump experiments [37], SN1987A [38], NA48/2 [39], BaBar [40] and NA64 [41].³ The light red region is excluded by the measurement of the electron anomalous magnetic moment. The green region can explain the discrepancy of muon anomalous magnetic moment with the Standard Model, but all the region is excluded by the other

²The constraint of dark matter direct detection can be evaded if χ splits into CP-even and CP-odd states since elastic scattering with nuclei does not occur in this case. Splitting the mass may be achieved by introducing additional scalar Σ' coupling with χ like $\Sigma'\chi^2$ since this term gives a mass splitting if the field Σ' gets a vacuum expectation value. As an concrete example of charge assignment, one can consider $Q_\Sigma = 1$, $Q_{\Sigma'} = 4/5$, $Q_S = -1/2$ and $Q_\chi = -2/5$.

³In our case, since the main decay mode of Z' would be $Z' \rightarrow sa \rightarrow e^+e^-aa$, the exclusion limits in Fig. 1 cannot directly be applied. However one can take these limits as conservative limits.

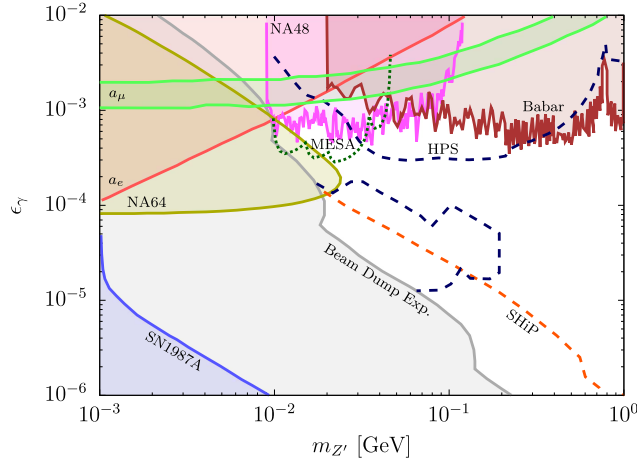


Figure 1: Current limits on the kinetic mixing ϵ_γ including beam dump experiments [37], SN1987A [38], NA48/2 [39], BaBar [40] and NA64 [41]. The dotted lines correspond to the future experiments: HPS [37], MESA [42] and SHiP [43].

limits. According to the plot, the upper limit on the kinetic mixing is roughly given by $\epsilon_\gamma \lesssim 10^{-3}$ for $m_{Z'} \gtrsim 10$ MeV. The Higgs mixing angle $\sin \alpha$ is also constrained by some experiments, and the strong bound $\sin \alpha \lesssim 0.01$ is given by B-meson decays when the second Higgs mass is $m_H \lesssim 5$ GeV [44]. Hereafter we fix the kinetic mixing parameter to be $\epsilon_\gamma = 5 \times 10^{-4}$ which can be explored by the HPS future experiment [37], and the Higgs mixing angle is also fixed to be $\sin \alpha = 10^{-3}$.

The hidden $U(1)_D$ gauge symmetry is broken by the vacuum expectation value of Σ . After the symmetry breaking, a pair of two particles (s, χ) or (a, χ) is stabilized by the residual $\mathbb{Z}_2 \times \mathbb{Z}'_2$ symmetry. Since $m_s > m_a$ because of the positive κ coupling that we assumed, a pair of a and χ can be stable dark matter particles, namely two-component dark matter. Furthermore, if the annihilation cross section for $\chi^\dagger \chi \rightarrow aa$ ($m_a < m_\chi$) is large enough, the lighter dark matter a is boosted at a region of high dark matter density (the Galactic centre for example). Such boosted dark matter can be detectable by large neutrino detectors such as Super-Kamiokande, IceCube, Hyper-Kamiokande, PINGU and DUNE. In the rest of the paper, we focus on the following mass interval and mass hierarchy

$$10 \text{ MeV} \lesssim m_a \lesssim m_H, \quad m_s \lesssim m_{Z'} \lesssim m_\chi \lesssim 10 \text{ GeV}, \quad (9)$$

in order to maximize possible signature of the boosted dark matter and obtain a large self-interacting cross section of the lighter dark matter a to improve the small scale structure problems such as cusp-vs-core problem, too-big-to-fail problem and missing satellite problem as we will discuss later.

The fraction of the heavier component of dark matter χ should be large to enhance the signals of the boosted dark matter via the annihilation $\chi^\dagger \chi \rightarrow aa$ while the fraction of the lighter component of dark matter a should also be large to improve the small scale

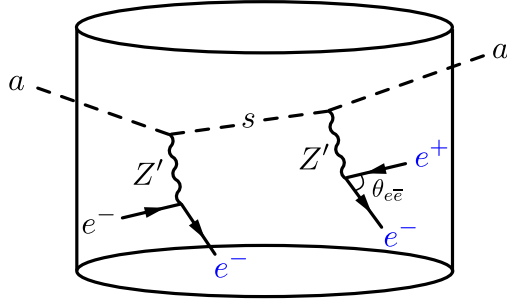


Figure 2: Two or three distinctive signals (electrons and positron) of the boosted dark matter a at Super-Kamiokande and Hyper-Kamiokande. The blue electron and position and its angle $\theta_{e\bar{e}}$ can be detected.

structure problems with a large self-interacting cross section. Therefore it is interesting to investigate the case that both components of dark matter are comparable. The concrete calculation of the relic abundance will be performed in Section 4, and we will concentrate on the parameter space such that each relic abundance $\Omega_\chi h^2$ and $\Omega_a h^2$ is in the range 40% \sim 60% of the observed total abundance which is taken as 3σ range of the PLANCK Collaboration $\Omega_\chi h^2 + \Omega_a h^2 = 0.1197 \pm 0.0022$ [1].

3 Signatures of the Boosted Dark Matter

In the non-relativistic limit, the thermally averaged annihilation cross section for $\chi^\dagger \chi \rightarrow aa$ is simply given by

$$\langle \sigma v \rangle_{\chi^\dagger \chi \rightarrow aa} = \frac{\lambda_{S\chi}^2}{64\pi m_\chi^2} \sqrt{1 - \frac{m_a^2}{m_\chi^2}}. \quad (10)$$

Note again the assumption of the scalar couplings $\lambda_{S\chi} \gg \lambda_{\Phi\chi}, \lambda_{\Sigma\chi}$ as our setup. The boosted dark matter a behaves as relativistic neutrinos and can be detectable with large size neutrino detectors via scattering with the electrons or protons in the detectors. In particular, the Super-Kamiokande Collaboration has recently investigated on the constraint of the boosted dark matter [45]. Hereafter we focus on scattering with electrons in water Cherenkov detectors since the expected number of events for proton scattering is rather smaller than that for electrons due to kinematics.

In principle, the CP-even state s is also produced by the annihilation $\chi^\dagger \chi \rightarrow ss$ with a similar production cross section of Eq. (10), and then the CP-even state s immediately decays into a . Thus the total energy distribution of the boosted dark matter a would be described by sum of those two contributions. However since energy of a for the latter case is rather small and is likely to be smaller than experimental energy threshold, we neglect

the contribution.⁴

The schematic picture in the detector is shown in Fig. 2. First, a boosted dark matter a comes in the detector, and the excited state s is produced by the inelastic scattering $ae^- \rightarrow se^-$. The produced s subsequently decays through the mode $s \rightarrow ae^+e^-$.⁵ If the decay length defined by $L_D \equiv \beta_s \gamma_s \tau_s$ is shorter than the detector length, multi-Cherenkov ring events can be observed where $\gamma_s = E_s/m_s$ is the boost factor, $\beta_s = |\mathbf{p}_s|/E_s$ is the velocity and $\tau_s \equiv \Gamma_{s \rightarrow ae^+e^-}^{-1}$ is the lifetime of the excited state s . The detector length (diameter of detector) is 39.3 m for Super-Kamiokande and 74 m for Hyper-Kamiokande. Furthermore if the angle between e^+ and e^- generated by the s decay ($\theta_{e\bar{e}}$ shown in Fig. 2) is larger than experimental threshold ($\theta_{e\bar{e}}^{\text{exp}} \gtrsim 3^\circ$) at Super-Kamiokande and Hyper-Kamiokande, a 3-Cherenkov ring event is expected to be observed. Otherwise, a 2-Cherenkov ring event is expected. These can be characteristic signals of non-minimal dark sector [23]. Note that although we do not consider scattering with a proton in this paper, an advantage of proton scattering is that the electron and positron induced by the decay $s \rightarrow ae^+e^-$ may be easily distinguishable since the angle between those particles are likely to be larger than the case of electron scattering due to rather small boost factor γ_s for proton scattering [20, 23].

We can roughly estimate the total number of multi-ring events which has been observed by Super-Kamiokande. From the literature [46], one can find that 3036 e -like multi-ring events have totally observed with 140.9 kiloton-year exposure. This is translated into 485 events per year at Super-Kamiokande. Among the total number of the events, only the events relevant to our multi-ring signals should be extracted by taking into account the direction, position and energy of the events in order to be compared with the prediction in the model. However since such detailed analysis of multi-Cherenkov ring events coming from Galactic centre at Super-Kamiokande has not been done, there is no substantial experimental bound for the boosted dark matter signals of multi-component dark matter.⁶

The differential cross section for the inelastic scattering $ae^- \rightarrow se^-$ mediated by Z' is computed as

$$\frac{d\sigma_{\text{inel}}}{dE_e} = \frac{m_e \overline{|\mathcal{M}_{\text{inel}}|^2}}{8\pi\lambda(s, m_a^2, m_e^2)}, \quad (11)$$

where s is the Manderstam variable related with the other variables t and u as $s + t + u = m_a^2 + m_s^2 + 2m_e^2$, $\lambda(x, y, z)$ is the kinematical function defined by $\lambda(x, y, z) = x^2 + y^2 + z^2 - 2xy - 2yz - 2zx$, E_e is the energy of the scattered electron and $\overline{|\mathcal{M}_{\text{inel}}|^2}$ is the squared amplitude spin averaged over initial state and summed over final state which is given by

$$\overline{|\mathcal{M}_{\text{inel}}|^2} = \frac{g_D^2 \epsilon_\gamma^2 \alpha_{\text{em}} \pi}{(t - m_{Z'}^2)^2} \left[(s - u)^2 - t^2 + 2t(m_s^2 + m_a^2) - (m_s^2 - m_a^2)^2 \right]. \quad (12)$$

⁴Taking into account the contribution of the s decay would be necessary if a more detailed phenomenological feature of the model is required to discriminate from the other models.

⁵Depending on the masses of a and s , another decay mode $s \rightarrow a\mu^+\mu^-$ may also be possible.

⁶We leave a systematic background analysis to the future work.

The Manderstam variable t is correlated with the scattered electron energy as $t = 2m_e(m_e - E_e)$. The total cross section is obtained by integrating Eq. (11) with respect to E_e . For a given energy s , the minimal and maximal E_e are given by

$$E_e^{\max} = \frac{(s - m_a^2 + m_e^2)(s - m_s^2 + m_e^2)}{4m_e s} + \frac{\sqrt{\lambda(s, m_a^2, m_e^2)}\sqrt{\lambda(s, m_s^2, m_e^2)}}{4m_e s}, \quad (13)$$

$$E_e^{\min} = \frac{(s - m_a^2 + m_e^2)(s - m_s^2 + m_e^2)}{4m_e s} - \frac{\sqrt{\lambda(s, m_a^2, m_e^2)}\sqrt{\lambda(s, m_s^2, m_e^2)}}{4m_e s}. \quad (14)$$

For comparison with Super-Kamiokande and Hyper-Kamiokande experiments, the experimental energy thresholds should be taken into account. The actual energy threshold of these experiments is $E_e^{\text{exp}} \gtrsim 0.01$ GeV. However since angular resolution is not so good for lower energy, we take a conservative lower energy threshold $E_e^{\text{exp}} > 0.1$ GeV [20].

The decay width for $s \rightarrow af\bar{f}$ mediated by off-shell Z' is calculated as

$$\Gamma_{s \rightarrow af\bar{f}} = \frac{g_D^2 \alpha_{\text{em}} \epsilon_\gamma^2}{192\pi^2 m_s^3} \int_{4m_f^2}^{(m_s - m_a)^2} \frac{\sqrt{(q^2 - m_s^2 - m_a^2)^2 - 4m_s^2 m_a^2}}{(q^2 - m_{Z'}^2)^2 + m_{Z'}^2 \Gamma_{Z'}^2} \sqrt{1 - \frac{4m_f^2}{q^2}} \left(1 + \frac{2m_f^2}{q^2}\right) dq^2, \quad (15)$$

where $q^2 \equiv (p_s - p_a)^2$ is transfer momentum of Z' , and $\Gamma_{Z'}$ is the total decay width of Z' which is given by

$$\begin{aligned} \Gamma_{Z'} = & \sum_f \frac{\alpha_{\text{em}} \epsilon_\gamma^2 m_{Z'}}{3} \left(1 + 2\frac{m_f^2}{m_{Z'}^2}\right) \sqrt{\lambda\left(1, \frac{m_f^2}{m_{Z'}^2}, \frac{m_f^2}{m_{Z'}^2}\right)} \\ & + \frac{g_D^2 m_{Z'}}{192\pi} \left[1 - 2\left(\frac{m_s^2}{m_{Z'}^2} + \frac{m_a^2}{m_{Z'}^2}\right) + \left(\frac{m_s^2}{m_{Z'}^2} - \frac{m_a^2}{m_{Z'}^2}\right)^2\right] \sqrt{\lambda\left(1, \frac{m_s^2}{m_{Z'}^2}, \frac{m_a^2}{m_{Z'}^2}\right)}, \end{aligned} \quad (16)$$

with the kinematical function $\lambda(x, y, z)$ defined above. The first term in Eq. (16) corresponds to the decay mode $Z' \rightarrow f\bar{f}$ and the second term is $Z' \rightarrow sa$. Since the kinetic mixing ϵ_γ is small, the decay width for $Z' \rightarrow f\bar{f}$ is suppressed and the contribution of $Z' \rightarrow sa$ becomes dominant if it is kinematically allowed.

The energy of the incoming boosted dark matter a denoted by E_a should be as large as

$$E_a > \frac{m_s^2 - m_a^2 + 2m_s m_e}{2m_e}, \quad (17)$$

so that the inelastic scattering $ae^- \rightarrow se^-$ can be kinematically accessible. The energy of the boosted dark matter is given by the mass of the heavier component dark matter ($E_a \approx m_\chi$) since the dark matter particles are non-relativistic. Eq. (17) implies that a larger energy E_a is kinematically required for scattering with electrons compared to that with protons because of the target particle mass in the denominator of Eq. (17) ($m_e \ll m_p$). On the other hand, if the energy of the initial state a is too large, the decay length of the excited state s tends to be too long to decay inside the detectors. Therefore

one can expect that relevant parameter space for multi-Cherenkov ring events is bounded from both below and above.

It is expected that the annihilation $\chi^\dagger\chi \rightarrow aa$ occurs at the Galactic centre, and the dark matter a is produced in all the directions. We take the dark matter flux only within 10° cone around the Galactic centre. In this case, the flux of the boosted dark matter a is estimated by [20]

$$\Phi_a^{10^\circ} = 9.9 \times 10^{-8} \text{ cm}^{-2}\text{s}^{-1} \left(\frac{\langle\sigma v\rangle_{\chi^\dagger\chi \rightarrow aa}}{5 \times 10^{-26} \text{ cm}^3/\text{s}} \right) \left(\frac{20 \text{ GeV}}{m_\chi} \right)^2 \left(\frac{\Omega_\chi}{\Omega_a + \Omega_\chi} \right)^2, \quad (18)$$

where the fraction of total relic abundance $\Omega_\chi/(\Omega_a + \Omega_\chi)$ is multiplied, and the Navarro-Frenk-White (NFW) dark matter profile is assumed [47]. The energy distribution of the scattered electron in the detector is given by [20]

$$E_e \frac{dN_{\text{inel}}}{dE_e} = \delta t N_{\text{target}} \Phi_a^{10^\circ} E_e \frac{d\sigma_{\text{inel}}}{dE_e}, \quad (19)$$

where δt is the exposure time, N_{target} is the number of target electrons in the detector which can be estimated as $N_{\text{target}} = 7.49 \times 10^{33}$ for Super-Kamiokande and $N_{\text{target}} = 1.25 \times 10^{35}$ for Hyper-Kamiokande from the fiducial volume 0.0224 megaton and $0.187 \times 2 = 0.374$ megaton (taking into account two 0.187 megaton tanks) [48], respectively. Integrating over the electron energy, the total expected number of events for the inelastic scattering is obtained.

Furthermore, we define the number of the (multi-)Cherenkov ring events in a specific region of interest as

$$N_{\text{signal}} = \delta t N_{\text{target}} \Phi_a^{10^\circ} \int_{E_e^{\min}}^{E_e^{\max}} dE_e \frac{d\sigma_{\text{inel}}}{dE_e} \text{Br}_{s \rightarrow ae\bar{e}} \int_{E_e'^{\min}}^{E_e'^{\max}} dE_e' \int_{E_{\bar{e}}^{\min}}^{E_{\bar{e}}^{\max}} dE_{\bar{e}} \int_{\theta_{e\bar{e}}^{\min}}^{\theta_{e\bar{e}}^{\max}} d\theta_{e\bar{e}} \frac{d^3 N_s}{dE_e' dE_{\bar{e}} d\theta_{e\bar{e}}}, \quad (20)$$

where $\text{Br}_{s \rightarrow ae\bar{e}}$ is the branching ratio of the decay $s \rightarrow ae^+e^-$ which is $\text{Br}_{s \rightarrow ae\bar{e}} = 1$ in our case, E_e' and $E_{\bar{e}}$ are the energy of the electron and positron produced by the decay of the boosted CP-even state s , and $d^3 N_s/dE_e' dE_{\bar{e}} d\theta_{e\bar{e}}$ is the energy and angular distribution of the electron and positron normalized to $N_s = 1$. In order to obtain the distribution $d^3 N_s/dE_e' dE_{\bar{e}} d\theta_{e\bar{e}}$ for the boosted state s , first we generate events of the s decay at rest frame with CalcHEP [49, 50], then each event is boosted by the Lorentz transformation.

4 The Constraints

4.1 Relic Abundance of Dark Matter

In general, one has to solve the coupled Boltzmann equation to calculate the relic abundance of the two-component dark matter. However since the masses of the dark

matter particles are hierarchical ($m_a \ll m_\chi$), the coupled Boltzmann equation can be simplified as follows

$$\frac{dn_\chi}{dt} + 3Hn_\chi = -\frac{\langle\sigma v\rangle_{\chi^\dagger\chi}}{2} (n_\chi^2 - n_\chi^{\text{eq}2}), \quad (21)$$

$$\frac{dn_a}{dt} + 3Hn_a = -\langle\sigma v\rangle_{aa} (n_a^2 - n_a^{\text{eq}2}), \quad (22)$$

where n_χ is the total number density of χ and χ^\dagger ,⁷ n_a is the dark matter number density of a , n_χ^{eq} and n_a^{eq} are the number densities in thermal equilibrium, H is the Hubble parameter, and $\langle\sigma v\rangle_{\chi^\dagger\chi}$ and $\langle\sigma v\rangle_{aa}$ are the total annihilation cross sections for each dark matter. These equations can be independently solved, and the total relic abundance should satisfy $\Omega_a h^2 + \Omega_\chi h^2 \approx 0.12$ observed by the PLANCK Collaboration [1].

The possible annihilation channels for χ dark matter are $\chi^\dagger\chi \rightarrow ss, aa, sa, HH, HZ', Z'Z', f\bar{f}$ where f is a Standard Model fermion and the relevant diagrams are shown in Fig. 3. Since we have assumed that $\lambda_{\Phi\chi}$ and $\lambda_{\Sigma\chi}$ are sub-dominant, some diagrams are negligible. In particular, the annihilation channel $\chi^\dagger\chi \rightarrow HH$ (the second line of Fig. 3) completely disappears in the case of $\lambda_{\Phi\chi} = \lambda_{\Sigma\chi} = 0$. In fact, this is required in order to be consistent with cosmic-ray and Cosmic Microwave Background (CMB) observations as we will see later. This is because if the annihilation cross section for the channel $\chi^\dagger\chi \rightarrow HH$ is large enough, the produced second Higgs boson H subsequently decays into e^+e^- . The other two channels $\chi^\dagger\chi \rightarrow Z'Z', HZ'$ should also be suppressed due to the same reason while the main decay channel of Z' is different ($Z' \rightarrow sa \rightarrow e^+e^-aa$). As a result, the coupling $|g_D Q_\chi|$ is strongly constrained. In addition, dark matter direct detection also gives strong constraint on $|g_D Q_\chi|$. Thus one can see that the main annihilation channel should eventually be $\chi^\dagger\chi \rightarrow ss, aa$ in the mass range given by Eq. (9). We use the public code micrOMEGAs to compute the relic abundance of χ [51].

For the lighter dark matter a , the relic abundance can be determined by the forbidden channel $aa \rightarrow HH$ where $m_a < m_H$.⁸ The relevant diagrams are shown in Fig. 4. In non-relativistic limit, the annihilation cross section for the forbidden channel is correlated with the inverse process $HH \rightarrow aa$ [54], and is given by

$$\langle\sigma v\rangle_{aa\rightarrow HH} = \frac{m_H}{32\pi m_a^3} \left| \lambda_{HHaa} - \frac{2\mu_{Haa}^2}{m_H^2} + \frac{\mu_{Haa}\mu_{HHH}}{3m_H^2 + im_H\Gamma_H} \right|^2 \sqrt{1 - \frac{m_a^2}{m_H^2}} e^{-2(m_H - m_a)/T}, \quad (23)$$

⁷Note that anti-dark matter particle χ^\dagger is different degree of freedom from dark matter χ . The number densities of χ and χ^\dagger can be regarded as exactly same assuming CP invariance. Because of this reason, the factor 1/2 appears in Eq. (21).

⁸The 3-to-2 process $aaa \rightarrow aH$ may give an impact on the computation of the relic abundance of a [52, 53].

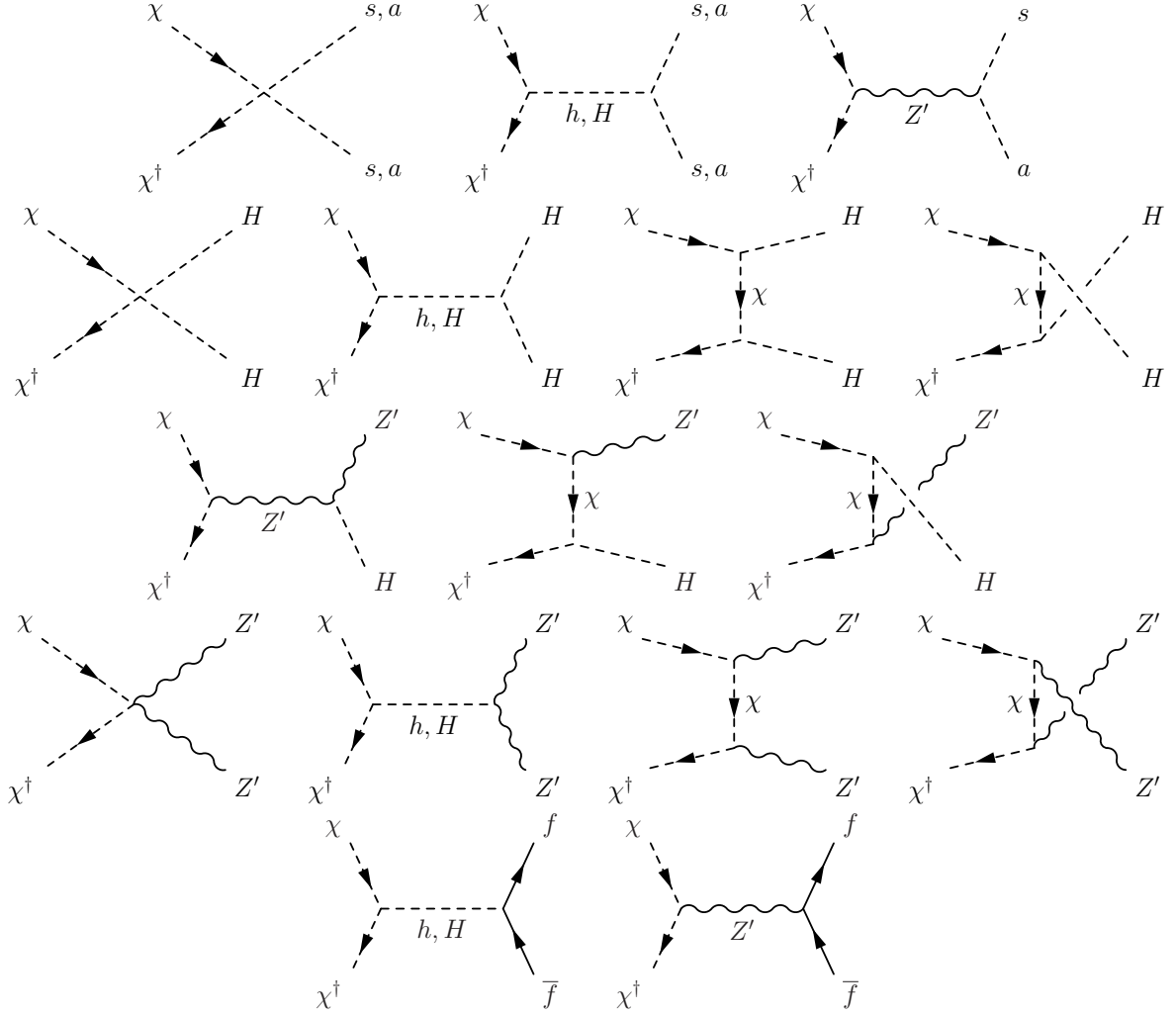


Figure 3: Complete diagrams for χ annihilations.

where T is temperature of the universe and the couplings λ_{HHaa} , μ_{Haa} μ_{HHH} are given by

$$\lambda_{HHaa} = \lambda_{\Phi S} \sin^2 \alpha + \lambda_{\Sigma S} \cos^2 \alpha, \quad (24)$$

$$\mu_{Haa} = -\sqrt{2}\lambda_{\Phi S}\langle\Phi\rangle \sin \alpha + \sqrt{2}\lambda_{\Sigma S}\langle\Sigma\rangle \cos \alpha - \frac{\kappa}{\sqrt{2}} \cos \alpha, \quad (25)$$

$$\begin{aligned} \mu_{HHH} = & \frac{3}{\sqrt{2}} \left(-\lambda_{\Phi}\langle\Phi\rangle \sin^3 \alpha + \lambda_{\Sigma}\langle\Sigma\rangle \cos^3 \alpha \right) \\ & + \frac{6}{\sqrt{2}} \lambda_{\Phi\Sigma} \sin \alpha \cos \alpha \left(-\langle\Phi\rangle \cos \alpha + \langle\Sigma\rangle \sin \alpha \right). \end{aligned} \quad (26)$$

For the H decay, the possible decay channel at tree level is $H \rightarrow f\bar{f}$ and $H \rightarrow aa$ if $m_H > 2m_a$ in our setup and the total decay width is given by

$$\Gamma_H = \sum_f \frac{y_f^2 m_H \sin^2 \alpha}{16\pi} \left(1 - 4 \frac{m_f^2}{m_H^2} \right)^{3/2} + \frac{\mu_{Haa}^2}{32\pi m_H} \sqrt{1 - \frac{4m_a^2}{m_H^2}}, \quad (27)$$

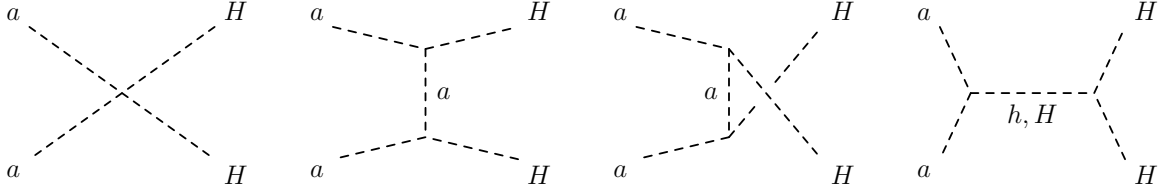


Figure 4: Complete diagrams for a annihilations. This annihilation is a forbidden channel due to $m_a < m_H$ but can occur with certain momentum in the early universe.

where y_f is the Yukawa coupling. The former term in Eq. (27) corresponds to the decay channel of $H \rightarrow f\bar{f}$ and the latter term is $H \rightarrow aa$. One can find that the cross section in Eq. (23) is exponentially suppressed if $(m_H - m_a)/T \gg 1$. The Boltzmann equation for the lighter dark matter a given by Eq. (22) is numerically solved and the relic abundance can be computed.

4.2 Direct Detection of Dark Matter

The current direct detection bounds and future sensitivities for dark matter mass range less than 10 GeV are summarized in the left plot of Fig. 5. The purple, green, blue, orange and yellow regions are already excluded by the experiments CRESST-II [55], CDMSlite [56], SuperCDMS [57], LUX [58], XENON1T [59], respectively. The blue dotted line represents the future sensitivity of SuperCDMS SNOLAB [60]. In the red region in the bottom, dark matter scattering cannot be distinguished from the elastic scattering with neutrinos (so-called neutrino floor).

The elastic scattering between the heavier dark matter χ and a proton is induced by the Z' boson via the gauge kinetic mixing ϵ_γ , and the spin independent cross section is computed as

$$\sigma_p^\chi = \frac{4Q_\chi^2 g_D^2 \alpha_{\text{em}} \epsilon_\gamma^2 m_p^2 m_\chi^2}{m_{Z'}^4 (m_p + m_\chi)^2}, \quad (28)$$

where $m_p = 938$ MeV is the proton mass. We define an effective scattering cross section $\sigma_p^{\chi \text{eff}} \equiv \sigma_p^\chi f_\chi$ to compare with the experimental bounds where $f_\chi \equiv \Omega_\chi / (\Omega_a + \Omega_\chi)$. This cross section is enhanced by the light mediator mass $m_{Z'}$ when $m_{Z'} \ll m_\chi$. Although the experimental direct detection bound for $m_\chi \lesssim 10$ GeV is rather weaker than that for the case of $m_\chi \gtrsim 10$ GeV, the constraint is strong enough since we are interested in the region of small mediator mass ($m_{Z'} \ll m_\chi$). With Eq. (28), the current upper bound on the elastic cross section can be translated into an upper bound on $|Q_\chi g_D|$ as shown in the right panel (purple lines) in Fig. 5 for $f_\chi = 0.5$. The upper bound depends on mass hierarchy $m_{Z'}/m_\chi$.

The dark matter χ can also scatter electron off with the same formula of the elastic cross section in Eq. (28) where m_p is replaced to m_e . The typical scale of the elastic cross section is $\sigma_e^\chi \lesssim \mathcal{O}(10^{-42})$ cm² while the current strongest upper bound given by XENON10

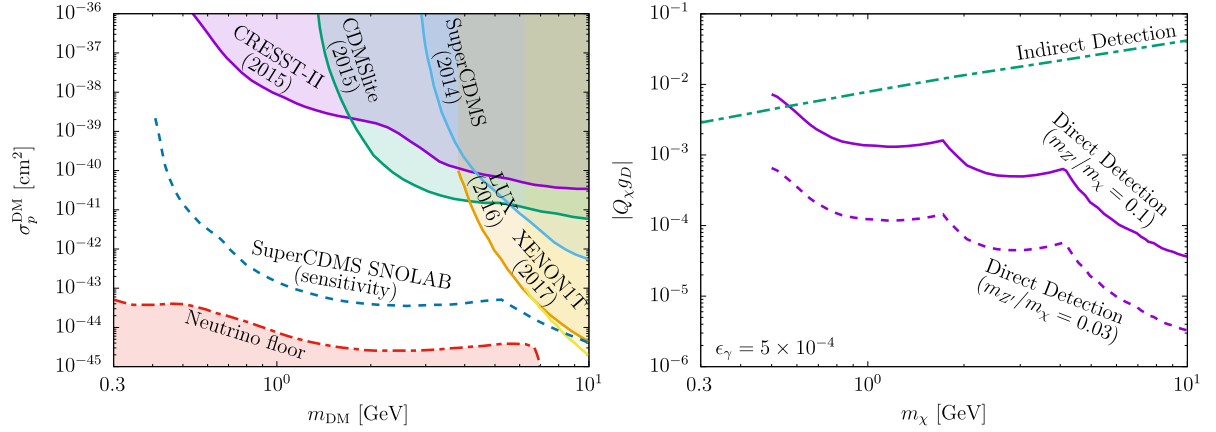


Figure 5: (Left): Current direct detection bounds (CRESST-II [55], CDMSlite [56], SuperCDMS [57], LUX [58], XENON1T [59]) and future sensitivities (SuperCDMS SNOLAB [60]). (Right): Bounds for the hidden $U(1)_D$ charge obtained from direct detection and indirect detection of the heavier component of dark matter for $f_\chi = 0.5$. The indirect detection bound is insensitive with the mass hierarchy $m_{Z'}/m_\chi$ unless χ and Z' are highly degenerate.

and XENON100 is $\sigma_e^{\text{exp}} = \mathcal{O}(10^{-38}) \text{ cm}^2$ at $\mathcal{O}(0.1) \text{ GeV}$ of dark matter mass [61]. Thus no substantial constraint is imposed from the scattering with electron.

For the lighter dark matter a , the elastic scattering cross section with a proton is very small since it is suppressed by the small reduced mass $(m_e^{-1} + m_a^{-1})^{-1}$. Note that Z' does not mediate for the lighter dark matter a unlike the χ dark matter. For the scattering with electron mediated by the Higgs bosons, the elastic scattering cross section is computed as

$$\sigma_e^a = \frac{m_e^4}{4\pi(m_e + m_a)^2} \left(\frac{\mu_{Haa} \sin \alpha}{m_H^2 \langle \Phi \rangle} - \frac{\mu_{haa} \cos \alpha}{m_h^2 \langle \Phi \rangle} \right)^2, \quad (29)$$

where μ_{Haa} and μ_{haa} are given in Eq. (25) and

$$\mu_{haa} = \sqrt{2}\lambda_{\Phi S} \langle \Phi \rangle \cos \alpha + \sqrt{2}\lambda_{\Sigma S} \langle \Sigma \rangle \sin \alpha - \frac{\kappa}{\sqrt{2}} \sin \alpha. \quad (30)$$

The magnitude of the cross section in our setup is roughly given by $\sigma_e^a \lesssim \mathcal{O}(10^{-43}) \text{ cm}^2$ which is small enough compared to the current experimental bound [61].

4.3 Cosmological Observations

4.3.1 Cosmic-ray, CMB and BBN Observations

In this model with our setup, the relevant annihilation channels to the cosmological observations are $\chi^\dagger \chi \rightarrow HZ'$ and $Z'Z'$. The channel $\chi^\dagger \chi \rightarrow HH$ is sufficiently suppressed by the assumption ($\lambda_{\Phi\chi}, \lambda_{\Sigma\chi} \ll 1$), and the channel $aa \rightarrow HH$ is kinematically forbidden in non-relativistic case since the momentum of dark matter is too small.

If H or Z' is produced by dark matter annihilations in the current times, these processes are constrained by gamma-ray and cosmic-ray observations since the produced particles H and Z' decay into charged particles. The dominant H decay channel is $H \rightarrow f\bar{f}$ whose decay width is given by the first term of Eq. (27). For Z' decay, the channel $Z' \rightarrow as$ is dominant, and the decay width is given by the second term of Eq. (16). Then s subsequently decays via $s \rightarrow ae^+e^-$, and gamma-rays are produced by Bremsstrahlung process and thus a constraint is imposed on the model [62].

In addition, after freeze-out of dark matter particles, at so-called dark ages, CMB is sensitively distorted by such non-standard production of charged particles and gamma-rays. As a result, it gives an upper bound on annihilation cross sections. Since the upper bound of annihilation cross sections depends on the energy spectrum of the produced e^+e^- , we take the strongest one as a conservative bound, which is roughly given by $\sigma v_{\chi^\dagger\chi \rightarrow Z'Z'} f_\chi^2 \lesssim (m_\chi/\text{GeV}) \times 10^{-27} \text{ cm}^3/\text{s}$ for $1 \text{ MeV} \lesssim m_\chi \lesssim 10 \text{ GeV}$ [63, 64]. Thus one can see that the upper bound becomes smaller than the value required for the correct relic abundance ($\sim 3 \times 10^{-26} \text{ cm}^3/\text{s}$) when $m_\chi \lesssim 30 \text{ GeV}$ and $f_\chi = 1$. In non-relativistic limit, the annihilation cross section for the channel $\chi^\dagger\chi \rightarrow Z'Z'$ is computed as

$$\sigma v_{\chi^\dagger\chi \rightarrow Z'Z'} = \frac{Q_\chi^4 g_D^4}{16\pi m_\chi^2} \sqrt{1 - \frac{m_{Z'}^2}{m_\chi^2}} \frac{16m_\chi^4 - 16m_\chi^2 m_{Z'}^2 + 3m_{Z'}^4}{(2m_\chi^2 - m_{Z'}^2)^2}, \quad (31)$$

which is velocity independent (s -wave). Therefore assuming $m_{Z'} \ll m_\chi$ in Eq. (31), one can translate it into an upper bound on the gauge coupling

$$|Q_\chi g_D| \lesssim 5.7 \times 10^{-3} \left(\frac{m_\chi}{\text{GeV}} \right)^{3/4} f_\chi^{-1/2}, \quad (32)$$

for our case. This bound implies that a milli-charge Q_χ for χ is necessary when $g_D = \mathcal{O}(1)$. This bound is shown as the green dot-dashed line in the right plot of Fig. 5.

For the channel $\chi^\dagger\chi \rightarrow HZ'$, the relevant diagram is only the left one in the third line of Fig. 3, and the annihilation cross section in non-relativistic limit is computed as

$$\sigma v_{\chi^\dagger\chi \rightarrow HZ'} = \frac{Q_\chi^2 g_D^4 \cos^2 \alpha}{4\pi} \frac{m_{Z'}^2 v^2}{(4m_\chi^2 - m_{Z'}^2)^2 + m_{Z'}^2 \Gamma_{Z'}^2} \left(1 + \frac{1}{3} \frac{m_\chi^2}{m_{Z'}^2} \right). \quad (33)$$

As one can find from Eq. (33), the annihilation cross section is velocity suppressed (p -wave). Thus this channel is sufficiently suppressed to evade the constraint of the cosmological observations.

Another annihilation channel $aa \rightarrow \gamma\gamma$ induced by the Higgs mixing also relevant to the constraints coming from the observations of gamma-rays and CMB. The current upper bound on the annihilation cross section is given by $\langle \sigma v \rangle_{\gamma\gamma} \lesssim 10^{-30} \text{ cm}^3/\text{s}$ for $10 \text{ MeV} \lesssim m_a \lesssim 100 \text{ MeV}$ [65, 66]. Although the annihilation cross section for this process sufficiently small compared to the current upper bound in most of parameter space if $\sin \alpha \lesssim 10^{-2}$ in our model, the cross section is enhanced in particular when the second Higgs mass is close to the resonance ($m_H \approx 2m_a$) as we will see benchmark

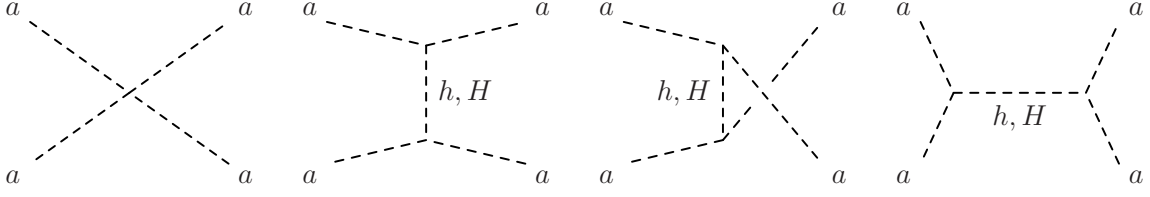


Figure 6: Diagrams for self-interacting cross section.

parameter sets in the following section. As a result, it gives a constraint on the Higgs mixing. In order to evade it, the mixing has been chosen to be $\sin \alpha = 10^{-3}$ in our analysis as mentioned earlier.

The successful Big Bang Nucleosynthesis (BBN) and the effective number of neutrinos (N_{eff}) are affected if freeze-out of dark matter occurs below $T \sim 1$ MeV scale. The constraints of the BBN and N_{eff} depend on annihilation channels. We impose the requirement of the freeze-out temperature $T_f \geq 1$ MeV as a conservative bound [67]. In our case, the annihilation channels $aa \rightarrow HH \rightarrow e^+e^+e^-e^-$ and $aa \rightarrow ss \rightarrow aae^+e^+e^-e^-$ would be relevant for the BBN and N_{eff} constraints. Since the freeze-out temperature of the channels $aa \rightarrow HH, ss$ are roughly given by $T_f \sim m_a/20$, this implies that $m_a \gtrsim 20$ MeV is imposed not to affect the successful BBN and the effective number of neutrinos.

4.3.2 Bullet Cluster

The self-interacting cross section for the dark matter a is computed from the diagrams in Fig. 6 as

$$\sigma_{\text{self}} = \frac{1}{128\pi m_a^2} \left| \frac{3}{2}\lambda_S - \frac{2\mu_{Haa}^2}{m_H^2} + \frac{\mu_{Haa}^2}{4m_a^2 - m_H^2 + im_H\Gamma_H} \right|^2, \quad (34)$$

where the contribution mediated by h is neglected. The self-interacting cross section for the heavier dark matter χ is much small and negligible even if the self-coupling λ_χ is $\mathcal{O}(1)$. The effective self-interacting cross section defined by $\sigma_{\text{self}}^{\text{eff}} \equiv \sigma_{\text{self}} f_a^2$ is bounded by the Bullet cluster observation which is given by $\sigma_{\text{self}}^{\text{eff}}/m_a \lesssim 1 \text{ cm}^2/\text{g}$ [68] where $f_a \equiv \Omega_a/(\Omega_a + \Omega_\chi)$ is the fraction of the lighter dark matter a .

On the other hand, the small scale structure problems can be improved with a large self-interacting cross section. The required magnitude of the effective self-interacting cross section is roughly $0.1 \lesssim \sigma_{\text{self}}^{\text{eff}}/m_a \lesssim 1 \text{ cm}^2/\text{g}$ [34, 35].

5 Numerical Analysis

5.1 Parameter scan

The following parameter range is considered for numerical analysis:

$$10 \text{ MeV} \leq m_a \leq 1 \text{ GeV}, \quad m_a \leq m_s \leq 10m_a, \quad m_a \leq m_H \leq 2m_a, \\ m_a + m_s \leq m_{Z'} \leq 3m_s, \quad m_{Z'} \leq m_\chi \leq 10 \text{ GeV}, \quad 10^{-3} \leq \lambda_{S\chi}, \lambda_{\Sigma S} \leq 1.$$

The other relevant parameters are fixed to be $g_D = 1$, $\epsilon_\gamma = 5 \times 10^{-4}$, $Q_\chi = 10^{-5}$ and $\sin \alpha = 10^{-3}$. The mass of the lighter component of dark matter a should be in the above range in order to induce a large self-interacting cross section for the small scale structure problems. The second extra Higgs boson mass should be in the above range for reproducing the relic abundance of dark matter a . The hidden gauge boson Z' should not be much heavier than s so that the decay length for the process $s \rightarrow ae^+e^-$ mediated by Z' becomes shorter than a detector size in order to see the multi-Cherenkov ring events. For the mass of dark matter χ , the mass range $m_\chi > 10 \text{ GeV}$ is not considered here since the constraint of dark matter direct detection becomes much stronger. The quartic coupling $\lambda_{S\chi}$ is a relevant parameter to the annihilation process $\chi^\dagger \chi \rightarrow aa$, and $\lambda_{\Sigma S}$ is relevant to the self-interacting cross section.

The decay length of s given by $L_D = \beta_s \gamma_s \tau_s$ should be shorter than the detector length so that the multi-Cherenkov ring events are observed as a characteristic signature of the non-minimal dark sector. We take a benchmark of the detector length as the diameter of Hyper-Kamiokande which is 74 m. Although the momentum of the excited state s produced by the inelastic scattering $ae^- \rightarrow se^-$ has a distribution, we assume the excited state s is produced with averaged momentum for each parameter set to make our discussion simple.

The parameter space consistent with all the constraints considered in the previous section (dark matter relic abundance, direct detection, cosmic-ray and cosmological observations) is shown in Fig. 7. For the dark matter relic abundance, we take 3σ range of the value observed by the PLANCK Collaboration $\Omega_\chi h^2 + \Omega_a h^2 = 0.1197 \pm 0.0022$ [1]. The left upper plot in Fig. 7 shows the parameter space in the plane $(m_a, m_H/m_a)$ where the mass range $m_a \leq 20 \text{ MeV}$ is excluded by the constraints of the BBN and N_{eff} . The purple (green) points represent the allowed parameter points with the decay length of s longer (shorter) than the detector length of Hyper-Kamiokande ($\sim 74 \text{ m}$). One can see that m_H is in the range $1.3 \lesssim m_H/m_a \lesssim 1.9$ to reproduce the correct range of the relic abundance Ω_a (40% \sim 60% of the total abundance) via the forbidden channel $aa \rightarrow HH$. The right upper plot shows the parameter space in the plane $(m_\chi, \lambda_{S\chi})$. The relic abundance of χ is almost determined by the quartic coupling $\lambda_{S\chi}$, and the coupling should be in the range of $10^{-4} \lesssim \lambda_{S\chi} \lesssim 10^{-2}$ to be consistent with the χ relic abundance. Furthermore, if the requirement of the decay length $L_D < 74 \text{ m}$ is imposed, the parameters should be in the range of $1 \text{ GeV} \lesssim m_\chi \lesssim 7 \text{ GeV}$ and $10^{-3} \lesssim \lambda_{S\chi} \lesssim 10^{-2}$. The left

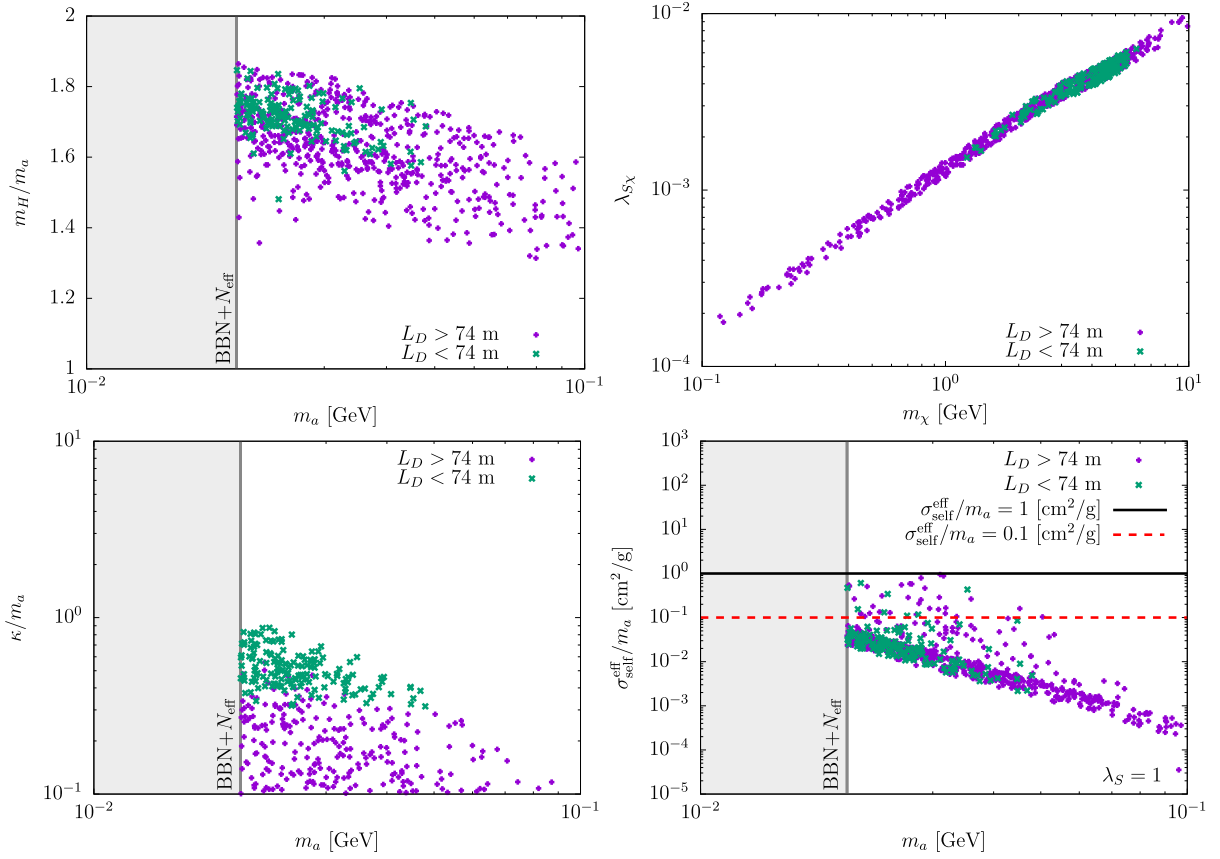


Figure 7: Parameter space allowed by all the constraints where $g_D = 1$, $\epsilon_\gamma = 5 \times 10^{-4}$, $Q_\chi = 10^{-5}$ and $\sin \alpha = 10^{-3}$

lower plot shows the parameter space in the plane of $(m_a, \kappa/m_a)$. One can see that a larger κ is required so that the decay length L_D can be shorter where the parameter κ is relevant to the mass splitting between s and a (see Eqs. (7) and (8)). The right lower plot shows the effective self-interacting cross section as a function of m_a where $\lambda_S = 1$. The large self-interacting cross section improving the small scale structure problems ($0.1 \text{ cm}^2/\text{g} \leq \sigma_{\text{self}}^{\text{eff}}/m_a \leq 1 \text{ cm}^2/\text{g}$) can be obtained when the dark matter mass is $m_a \lesssim 50 \text{ MeV}$.

With these allowed parameter sets, the annihilation cross section boosting the lighter dark matter a is shown as a function of m_χ in the left panel of Fig. 8. The order of the magnitude spreads in the range $4 \times 10^{-26} \text{ cm}^3/\text{s} \lesssim \langle \sigma v \rangle_{\chi^\dagger \chi \rightarrow aa} \lesssim 1.5 \times 10^{-25} \text{ cm}^3/\text{s}$, and one can see that this process is dominant to determine the relic abundance of the heavier dark matter χ . In the right panel of Fig. 8, the effective elastic cross section $\sigma_p^{\chi \text{ eff}}$ for direct detection of dark matter is shown as a function of m_χ . All the parameter sets with $L_D < 74 \text{ m}$ can be explored by the future direct detection experiment SuperCDMS SNOLAB [60] even though the hidden $U(1)_D$ charge is small as $Q_\chi = 10^{-5}$.

With the parameter sets satisfying $L_D < 74 \text{ m}$, the number of multi-Cherenkov ring

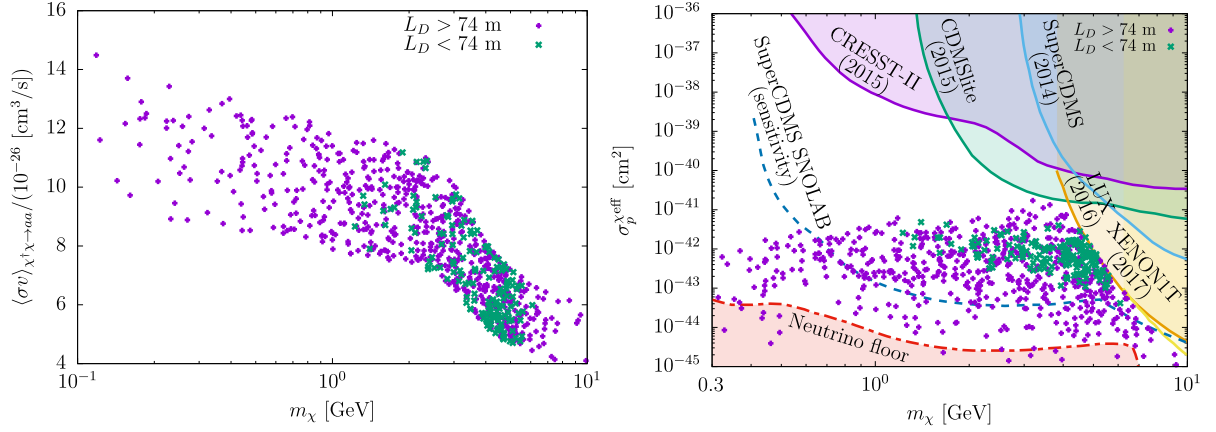


Figure 8: (Left): annihilation cross section boosting the dark matter a . (Right): effective elastic scattering cross section for direct detection of the dark matter χ where $g_D = 1$, $\epsilon_\gamma = 5 \times 10^{-4}$, $Q_\chi = 10^{-5}$ and $\sin \alpha = 10^{-3}$. The same parameter sets are used with Fig. 7.

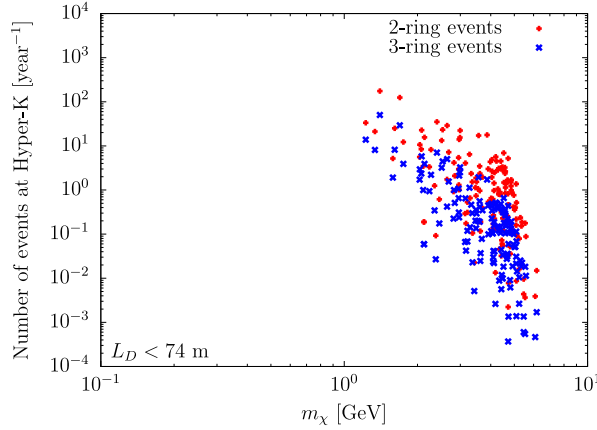


Figure 9: Expected number of the multi-Cherenkov ring events at Hyper-Kamiokande where $g_D = 1$, $\epsilon_\gamma = 5 \times 10^{-4}$, $Q_\chi = 10^{-5}$ and $\sin \alpha = 10^{-3}$.

events at Hyper-Kamiokande is plotted as a function of m_χ in Fig. 9 where the experimental energy threshold $E_e, E'_e, E_{\bar{e}} > 0.1 \text{ GeV}$ is imposed. The blue points correspond to the number of 3-Cherenkov ring events with the experimental angular threshold $\theta_{e\bar{e}} \geq 3^\circ$ while the red points correspond to the number of 2-Cherenkov ring events with $\theta_{e\bar{e}} < 3^\circ$. One can see from Fig. 9 that $\mathcal{O}(100)$ multi-Cherenkov ring events per year can be expected at most. However if one requires a large self-interaction for the small scale structure problems, the expected number of events would decrease.

Table 2: Benchmark parameter sets where $g_D = 1$, $\epsilon_\gamma = 5 \times 10^{-4}$, $\sin \alpha = 10^{-3}$ and $Q_\chi = 10^{-5}$.

	m_a [MeV]	m_s [MeV]	m_χ [GeV]	$m_{Z'}$ [MeV]	m_H [MeV]	$\lambda_{S\chi}$	$\lambda_{\Sigma S}$
BM1	21.0	60.3	4.86	102	38.4	5.35×10^{-3}	0.251
BM2	24.2	49.1	2.27	75.3	44.5	3.17×10^{-3}	0.516
BM3	28.0	48.8	2.99	78.3	50.5	3.34×10^{-3}	0.609
BM4	23.8	54.3	4.60	96.4	43.1	4.42×10^{-3}	0.386

Table 3: Prediction with the benchmark parameter sets in Tab. 2.

	$\Omega_a h^2 : \Omega_\chi h^2$	$\sigma_p^{\chi\text{eff}}$ [cm ²]	L_D [m]	$\langle \sigma v \rangle_{\chi^\dagger \chi \rightarrow aa}$ [cm ³ /s]	$\sigma_{\text{self}}^{\text{eff}}/m_a$ [cm ² /g]
BM1	59.0% : 41.0%	6.43×10^{-43}	17.9	6.75×10^{-26}	0.155
BM2	58.4% : 41.6%	1.62×10^{-42}	22.4	1.09×10^{-25}	0.344
BM3	45.4% : 54.6%	2.10×10^{-42}	67.0	7.11×10^{-26}	0.117
BM4	44.8% : 55.2%	1.10×10^{-42}	41.1	5.15×10^{-26}	0.132

5.2 Benchmark Points

We choose some benchmark (BM) parameter sets from the above analysis as shown in Tab. 2. One can see that the scale of the Z' mass is $m_{Z'} \lesssim 100$ MeV, and the coupling $\lambda_{\Sigma S}$ is $\lambda_{\Sigma S} = \mathcal{O}(0.1)$. With these parameter sets, the predicted physical quantities such as relic abundance and cross sections are summarized in Tab. 3. These parameter sets can improve the small scale structure problems with $0.1 \text{ cm}^2/\text{g} < \sigma_{\text{self}}^{\text{eff}}/m_a < 1 \text{ cm}^2/\text{g}$. In the left column of Tab. 4, the numbers of the total inelastic scattering events without any cuts are listed. For each parameter set, the energy and angular distributions of the electrons are shown in Fig. 10 where the left is $E_e d\sigma_{\text{inel}}/dE_e$ and the right is $dN_s/d\theta_{e\bar{e}}$. One can see that the inelastic cross section σ_{inel} is relatively small for BM2 (left plot), however the total expected number of events in Tab. 4 is relatively large due to the small χ mass (Tab. 2) and the large annihilation cross section $\langle \sigma v \rangle_{\chi^\dagger \chi \rightarrow aa}$ (Tab. 3). In the centre and right columns of Tab. 4, the number of 2-Cherenkov ring events ($E_e, E'_e, E_{\bar{e}} > 0.1$ GeV and $\theta_{e\bar{e}} < 3^\circ$) and 3-Cherenkov ring events ($E_e, E'_e, E_{\bar{e}} > 0.1$ GeV and $\theta_{e\bar{e}} \geq 3^\circ$) are summarized. In particular, a few 3-Cherenkov ring events per year can be expected for BM2 and BM3.⁹

⁹These numbers of events have been estimated assuming the NFW dark matter profile, and would increase with a few factor if a more cusp profile is considered such as Einasto profile [69].

Table 4: Expected number of the multi-Cherenkov ring events at Hyper-Kamiokande for the benchmark parameter sets in Tab. 2.

	Total events [year ⁻¹]	2-ring events [year ⁻¹]	3-ring events [year ⁻¹]
BM1	1.61	0.98	0.113
BM2	21.9	8.21	2.21
BM3	28.6	15.5	2.52
BM4	4.20	2.64	0.266

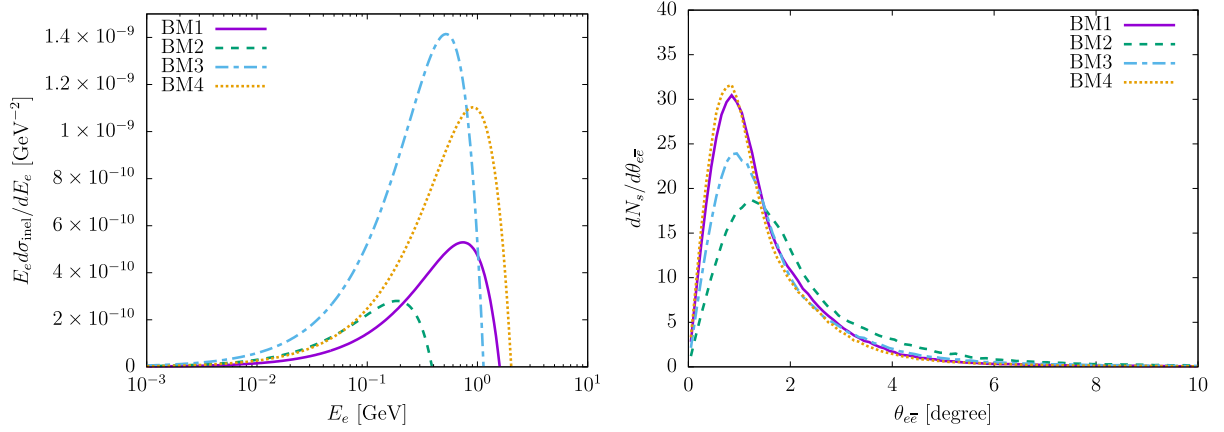


Figure 10: Energy and angular distributions for BM1-BM4.

6 Summary and Conclusions

We have constructed a model extended by three new scalar fields with a hidden $U(1)_D$ gauge symmetry where one of the new scalar has a milli-charge of $U(1)_D$ symmetry. The residual symmetry $\mathbb{Z}_2 \times \mathbb{Z}'_2$ remains after the spontaneous breaking of the hidden $U(1)_D$ gauge symmetry, which guarantees two stable particles in the model. Thus the model has two-component dark matter.

In this model, characteristic signatures of the boosted dark matter are induced. Namely, the multi-Cherenkov ring events are expected to be observed at large neutrino detectors such as Super-Kamiokande and Hyper-Kamiokande. Taking into account the relevant constraints such as dark matter relic abundance, direct detection, cosmic-ray and cosmological observations, we have explored allowed parameter space in the specific mass interval from 10 MeV to 10 GeV. With the allowed parameter sets, we have estimated the number of multi-Cherenkov ring events at Hyper-Kamiokande future experiment. Our benchmark parameter sets have shown that $\mathcal{O}(100)$ multi-Cherenkov events per year are expected at most. Moreover, if one requires a large self-interacting cross section of the lighter component of dark matter a to improve the small scale structure problems, 3-Cherenkov ring events decrease to a few events per year.

The mass scale of the hidden gauge boson Z' has been required to be $m_{Z'} \lesssim 100$ MeV so that the decay length is shorter than the detector length. Such light Z' can be tested by the HPS future experiment. Since the Z' gauge boson is light enough, the elastic scattering cross section for $\chi p^+ \rightarrow \chi p^+$ has been enhanced. As a result, the dark matter χ with $m_\chi = \mathcal{O}(1)$ GeV can be detectable by the future dark matter direct detection experiment SuperCDMS SNOLAB in spite of the small charge of hidden $U(1)_D$ gauge symmetry.

Acknowledgments

M. A. thank Doojin Kim, Jong-Chul Park, and Seodong Shin for early discussions about inelastic boosted dark matter. M. A. also thank Yoshinari Hayato for helpful discussions on Super-Kamiokande experiments. M. A. is supported in part by the Japan Society for the Promotion of Sciences (JSPS) Grant-in-Aid for Scientific Research (Grant No. 25400250 and No. 16H00864). T. T. acknowledges support from JSPS Fellowships for Research Abroad.

References

- [1] P. A. R. Ade *et al.* [Planck Collaboration], *Astron. Astrophys.* **594**, A13 (2016) [[arXiv:1502.01589](#) [astro-ph.CO]].
- [2] Z. G. Berezhiani and M. Y. Khlopov, *Z. Phys. C* **49**, 73 (1991).
- [3] C. Boehm, P. Fayet and J. Silk, *Phys. Rev. D* **69**, 101302 (2004) [[hep-ph/0311143](#)].
- [4] D. Chialva, P. S. B. Dev and A. Mazumdar, *Phys. Rev. D* **87**, no. 6, 063522 (2013) [[arXiv:1211.0250](#) [hep-ph]].
- [5] M. Aoki, J. Kubo and H. Takano, *Phys. Rev. D* **87**, no. 11, 116001 (2013) [[arXiv:1302.3936](#) [hep-ph]].
- [6] Y. Kajiyama, H. Okada and T. Toma, *Phys. Rev. D* **88**, no. 1, 015029 (2013) [[arXiv:1303.7356](#) [hep-ph]].
- [7] S. Bhattacharya, A. Drozd, B. Grzadkowski and J. Wudka, *JHEP* **1310**, 158 (2013) [[arXiv:1309.2986](#) [hep-ph]].
- [8] S. Esch, M. Klasen and C. E. Yaguna, *JHEP* **1409**, 108 (2014) [[arXiv:1406.0617](#) [hep-ph]].
- [9] M. Aoki, J. Kubo and H. Takano, *Phys. Rev. D* **90**, no. 7, 076011 (2014) [[arXiv:1408.1853](#) [hep-ph]].
- [10] A. Karam and K. Tamvakis, *Phys. Rev. D* **94**, no. 5, 055004 (2016) [[arXiv:1607.01001](#) [hep-ph]].

- [11] S. Bhattacharya, P. Poulose and P. Ghosh, JCAP **1704**, no. 04, 043 (2017) [[arXiv:1607.08461](#) [hep-ph]].
- [12] A. DiFranzo and G. Mohlabeng, JHEP **1701**, 080 (2017) [[arXiv:1610.07606](#) [hep-ph]].
- [13] G. Arcadi, C. Gross, O. Lebedev, Y. Mambrini, S. Pokorski and T. Toma, JHEP **1612**, 081 (2016) [[arXiv:1611.00365](#) [hep-ph]].
- [14] D. Borah, A. Dasgupta, U. K. Dey, S. Patra and G. Tomar, JHEP **1709**, 005 (2017) [[arXiv:1704.04138](#) [hep-ph]].
- [15] S. Bhattacharya, P. Ghosh, T. N. Maity and T. S. Ray, JHEP **1710**, 088 (2017) [[arXiv:1706.04699](#) [hep-ph]].
- [16] A. Ahmed, M. Duch, B. Grzadkowski and M. Iglicki, [arXiv:1710.01853](#) [hep-ph].
- [17] M. Aoki, D. Kaneko and J. Kubo, Front. in Phys. **5**, 53 (2017) [[arXiv:1711.03765](#) [hep-ph]].
- [18] J. Fan, A. Katz, L. Randall and M. Reece, Phys. Dark Univ. **2**, 139 (2013) [[arXiv:1303.1521](#) [astro-ph.CO]].
- [19] J. Fan, A. Katz, L. Randall and M. Reece, Phys. Rev. Lett. **110**, no. 21, 211302 (2013) [[arXiv:1303.3271](#) [hep-ph]].
- [20] K. Agashe, Y. Cui, L. Necib and J. Thaler, JCAP **1410**, no. 10, 062 (2014) [[arXiv:1405.7370](#) [hep-ph]].
- [21] K. Kong, G. Mohlabeng and J. C. Park, Phys. Lett. B **743**, 256 (2015) [[arXiv:1411.6632](#) [hep-ph]].
- [22] H. Alhazmi, K. Kong, G. Mohlabeng and J. C. Park, JHEP **1704**, 158 (2017) [[arXiv:1611.09866](#) [hep-ph]].
- [23] D. Kim, J. C. Park and S. Shin, Phys. Rev. Lett. **119**, no. 16, 161801 (2017) [[arXiv:1612.06867](#) [hep-ph]].
- [24] G. F. Giudice, D. Kim, J. C. Park and S. Shin, Phys. Lett. B **780**, 543 (2018) [[arXiv:1712.07126](#) [hep-ph]].
- [25] A. Chatterjee, A. De Roeck, D. Kim, Z. G. Moghaddam, J. C. Park, S. Shin, L. H. Whitehead and J. Yu, [arXiv:1803.03264](#) [hep-ph].
- [26] D. Kim, K. Kong, J. C. Park and S. Shin, [[arXiv:1804.07302](#) [hep-ph]].
- [27] M. R. Dziomba, “A Study of neutrino Oscillation Models with Super-Kamiokande Atmospheric Neutrino Data”.
- [28] Y. Ashie *et al.* [Super-Kamiokande Collaboration], Phys. Rev. D **71**, 112005 (2005) [[hep-ex/0501064](#)].
- [29] R. Abbasi *et al.* [IceCube Collaboration], Phys. Rev. D **84**, 022004 (2011) [[arXiv:1101.3349](#) [astro-ph.HE]].

- [30] M. G. Aartsen *et al.* [IceCube Collaboration], Phys. Rev. D **89**, no. 10, 102001 (2014) [[arXiv:1312.0104](#) [astro-ph.HE]].
- [31] E. Kearns *et al.* [Hyper-Kamiokande Working Group], [arXiv:1309.0184](#) [hep-ex].
- [32] M. G. Aartsen *et al.* [IceCube PINGU Collaboration], [arXiv:1401.2046](#) [physics.ins-det].
- [33] R. Acciarri *et al.* [DUNE Collaboration], [arXiv:1512.06148](#) [physics.ins-det].
- [34] O. D. Elbert, J. S. Bullock, S. Garrison-Kimmel, M. Rocha, J. Oñorbe and A. H. G. Peter, Mon. Not. Roy. Astron. Soc. **453**, no. 1, 29 (2015) [[arXiv:1412.1477](#) [astro-ph.GA]].
- [35] S. Tulin and H. B. Yu, Phys. Rept. **730**, 1 (2018) [[arXiv:1705.02358](#) [hep-ph]].
- [36] M. Aoki and T. Toma, JCAP **1701**, no. 01, 042 (2017) [[arXiv:1611.06746](#) [hep-ph]].
- [37] R. Essig *et al.*, [arXiv:1311.0029](#) [hep-ph].
- [38] D. Kazanas, R. N. Mohapatra, S. Nussinov, V. L. Teplitz and Y. Zhang, Nucl. Phys. B **890**, 17 (2014) [[arXiv:1410.0221](#) [hep-ph]].
- [39] J. R. Batley *et al.* [NA48/2 Collaboration], Phys. Lett. B **746**, 178 (2015) [[arXiv:1504.00607](#) [hep-ex]].
- [40] J. P. Lees *et al.* [BaBar Collaboration], Phys. Rev. Lett. **113**, no. 20, 201801 (2014) [[arXiv:1406.2980](#) [hep-ex]].
- [41] D. Banerjee *et al.* [NA64 Collaboration], Phys. Rev. Lett. **120**, no. 23, 231802 (2018) [[arXiv:1803.07748](#) [hep-ex]].
- [42] T. Beranek, H. Merkel and M. Vanderhaeghen, Phys. Rev. D **88**, 015032 (2013) [[arXiv:1303.2540](#) [hep-ph]].
- [43] S. Alekhin *et al.*, Rept. Prog. Phys. **79**, no. 12, 124201 (2016) [[arXiv:1504.04855](#) [hep-ph]].
- [44] A. Falkowski, C. Gross and O. Lebedev, JHEP **1505**, 057 (2015) [[arXiv:1502.01361](#) [hep-ph]].
- [45] C. Kachulis *et al.* [Super-Kamiokande Collaboration], Phys. Rev. Lett. **120**, no. 22, 221301 (2018) [[arXiv:1711.05278](#) [hep-ex]].
- [46] H. Nishino *et al.* [Super-Kamiokande Collaboration], Phys. Rev. Lett. **102**, 141801 (2009) [[arXiv:0903.0676](#) [hep-ex]].
- [47] J. F. Navarro, C. S. Frenk and S. D. M. White, Astrophys. J. **462**, 563 (1996) [[astro-ph/9508025](#)].
- [48] K. Abe *et al.* [Hyper-Kamiokande Collaboration], [arXiv:1805.04163](#) [physics.ins-det].
- [49] A. Pukhov *et al.*, [hep-ph/9908288](#).

- [50] A. Pukhov, [hep-ph/0412191](#).
- [51] G. Bélanger, F. Boudjema, A. Pukhov and A. Semenov, *Comput. Phys. Commun.* **192**, 322 (2015) [[arXiv:1407.6129](#) [hep-ph]].
- [52] U. K. Dey, T. N. Maity and T. S. Ray, *JCAP* **1703**, no. 03, 045 (2017) [[arXiv:1612.09074](#) [hep-ph]].
- [53] J. M. Cline, H. Liu, T. Slatyer and W. Xue, *Phys. Rev. D* **96**, no. 8, 083521 (2017) [[arXiv:1702.07716](#) [hep-ph]].
- [54] R. T. D’Agnolo and J. T. Ruderman, *Phys. Rev. Lett.* **115**, no. 6, 061301 (2015) [[arXiv:1505.07107](#) [hep-ph]].
- [55] G. Angloher *et al.* [CRESST Collaboration], *Eur. Phys. J. C* **76**, no. 1, 25 (2016) [[arXiv:1509.01515](#) [astro-ph.CO]].
- [56] R. Agnese *et al.* [SuperCDMS Collaboration], *Phys. Rev. Lett.* **116**, no. 7, 071301 (2016) [[arXiv:1509.02448](#) [astro-ph.CO]].
- [57] R. Agnese *et al.* [SuperCDMS Collaboration], *Phys. Rev. Lett.* **112**, no. 24, 241302 (2014) [[arXiv:1402.7137](#) [hep-ex]].
- [58] D. S. Akerib *et al.* [LUX Collaboration], *Phys. Rev. Lett.* **116**, no. 16, 161301 (2016) [[arXiv:1512.03506](#) [astro-ph.CO]].
- [59] E. Aprile *et al.* [XENON Collaboration], *Phys. Rev. Lett.* **119**, no. 18, 181301 (2017) [[arXiv:1705.06655](#) [astro-ph.CO]].
- [60] R. Agnese *et al.* [SuperCDMS Collaboration], *Phys. Rev. D* **95**, no. 8, 082002 (2017) [[arXiv:1610.00006](#) [physics.ins-det]].
- [61] R. Essig, T. Volansky and T. T. Yu, *Phys. Rev. D* **96**, no. 4, 043017 (2017) [[arXiv:1703.00910](#) [hep-ph]].
- [62] R. Essig, E. Kuflik, S. D. McDermott, T. Volansky and K. M. Zurek, *JHEP* **1311**, 193 (2013) [[arXiv:1309.4091](#) [hep-ph]].
- [63] T. R. Slatyer, *Phys. Rev. D* **93**, no. 2, 023527 (2016) [[arXiv:1506.03811](#) [hep-ph]].
- [64] H. Liu, T. R. Slatyer and J. Zavala, *Phys. Rev. D* **94**, no. 6, 063507 (2016) [[arXiv:1604.02457](#) [astro-ph.CO]].
- [65] K. K. Boddy and J. Kumar, *Phys. Rev. D* **92**, no. 2, 023533 (2015) [[arXiv:1504.04024](#) [astro-ph.CO]].
- [66] R. Bartels, D. Gaggero and C. Weniger, *JCAP* **1705**, no. 05, 001 (2017) [[arXiv:1703.02546](#) [astro-ph.HE]].
- [67] C. Boehm, M. J. Dolan and C. McCabe, *JCAP* **1308**, 041 (2013) [[arXiv:1303.6270](#) [hep-ph]].
- [68] S. W. Randall, M. Markevitch, D. Clowe, A. H. Gonzalez and M. Bradac, *Astrophys. J.* **679**, 1173 (2008) [[arXiv:0704.0261](#) [astro-ph]].

- [69] M. Cirelli *et al.*, JCAP **1103**, 051 (2011) Erratum: [JCAP **1210**, E01 (2012)] [[arXiv:1012.4515](#) [hep-ph]].